Heliyon

Received:
22 December 2018
Revised:
9 March 2019
Accepted:
20 March 2019

Cite as:
Damian C. Onwudiwe.
Microwave-assisted synthesis of PbS nanostructures.
Heliyon 5 (2019) e01413.
doi: 10.1016/j.heliyon.2019.e01413

Microwave-assisted synthesis of PbS nanostructures

Damian C. Onwudiwe [a,b,*]

[a] *Material Science Innovation and Modelling (MaSIM) Research Focus Area, Faculty of Natural and Agricultural Sciences, North-West University, Mafikeng Campus, Private Bag X2046, Mmabatho 2735, South Africa*

[b] *Department of Chemistry, School of Physical and Chemical Sciences, Faculty of Natural and Agricultural Sciences, North-West University, Mafikeng Campus, Private Bag X2046, Mmabatho 2735, South Africa*

[*] Corresponding author.

E-mail address: Damian.Onwudiwe@nwu.ac.za (D.C. Onwudiwe).

Abstract

The synthesis of PbS nanostructures by microwave irradiation of single source precursor compounds in ethyleneglycol medium is reported. Pb(II) bis(*N*-ethyl-*N*-phenyldithiocarbamate) and Pb(II) bis(*N*-butyl-*N*-phenyldithiocarbamate) represented as complexes (**1**) and (**2**) respectively were utilised. The prepared PbS nanostructures were characterized using X-ray diffraction (XRD), Transmission electron microscopy (TEM), and absorption spectroscopy. The results showed that complex (**1**) can project the formation of nanorod with (111) basal plane, while (**2**) project the formation of nanocube with (001) basal plane. The formation of different morphologies in ethylene glycol may also be due to the selective binding to specific crystallite facets of the PbS through the hydroxyl groups of ethylene glycol. In the nanorod, the selective stabilization of the (111) face of PbS, resulted in anisotropic growth along the (100) face. The high resolution TEM images showed distinct lattice fringes which confirmed the crystallinity of the nanostructures. The band gap energies were obtained as 1.10 and 1.12 eV for the nanorods and nanocubes respectively, a significant blue shift from the bulk value (0.4 eV) which could be ascribed to quantum confinement effect. The result established the significant effect of the precursor type on the morphologies of the PbS.

Keyword: Materials chemistry

https://doi.org/10.1016/j.heliyon.2019.e01413

1. Introduction

Semiconductor metal sulphides with sizes in the nanometer dimensions have been the focus of recent research interest. The unique properties of these form of materials are fundamentally based on quantum size effect which governs the behaviour of nanosized semiconductors [1, 2, 3]. Lead sulphide is an important direct semiconductor which belongs to the IV-VI group. It has drawn considerable interest due to its small direct bandgap (0.41 eV) which, coupled with its large exciton Bohr radius (18 nm) and high dielectric constant [4], has the prospect of being applied in different optical and photonic fields [5]. It is possible to vary the optical band gap from 0.41 eV to values up to 13 times higher by varying the size from bulk to nanoparticles [6]. Potential areas of application include in photonic materials [7], thermoelectric devices [8], Pb^{II} ion-selective sensor, photographic equipment, and solar cells [9].

As diverse areas of applications of semiconductor nanoparticles continue to emerge, research into different methods of their synthesis becomes a vibrant area in materials chemistry. Several approaches have been reported for the synthesis of PbS nanoparticles such as sonochemical method [10], thermal decomposition [11], chemical bath deposition [12], irradiation by gamma rays [13] or UV rays [14], and also the use of microbes [15]. The different synthesis routes generate PbS of different morphologies which have effects on the materials properties.

Microwave synthesis has been employed in the synthesis of nanoparticles as it combines the advantage of speed and homogeneous heating of the precursor materials. Microwave irradiation has a penetration characteristic, which makes it possible to homogeneously heat up the reaction solution. The result is uniform nucleation and rapid crystal growth, which lead to the formation of crystallites that has narrow size distribution [16]. Compared to other conventional methods, synthesis by microwave irradiation has the advantage of short time of reaction, which is ascribed to the combined forces created by both electric and magnetic components of the microwave that generates friction and collisions of the molecules [1]. The synthesis of PbS nanoparticles by microwave irradiation method usually involves a lead salt and sulphur sources. Using this approach PbS obtained from $Pb(NO_3)_2$ and $Pb(Ac)_2$, as the lead sources, and different sulphur sources such as sulphur powder, thioacetamide and thiourea, have been reported [1, 17, 18, 19]. However, the use of a single compound which contains all the elements required in the final product has the advantage of simplicity, safety and mildness. Sun *et al.* [20], have reported the microwave-assisted preparation of PbS nanocrystals using lead diethyldithiocarbamate. This indicates the possibility of obtaining PbS nanoparticles from single-source molecular precursor compounds by microwave irradiation. Dithiocarbamates have interesting chemistry and applications. Pb(II) bis(*N*-ethyl-*N*-phenyl

https://doi.org/10.1016/j.heliyon.2019.e01413

dithiocarbamate) has been used in the rubber industry as vulcanising agent [21]. The wide application of metal dithiocarbamates in materials synthesis is associated with the ability to modify the materials properties by altering the substituent group on the nitrogen atoms. Different structural motifs have generated a wide array of isotropic and anisotropic nanomaterials [22, 23, 24]. Generally, the use of Pb(II) dithiocarbamate complexes as single source precursors (SSPs) to PbS nanoparticles have advantages over other Pb complexes that also contain ligands which have metal to sulphur bonds such as thiourea and xanthate. Although, these complexes show high solid state thermal stability and are able to form PbS nanoparticles upon thermal decomposition [25, 26], dithiocarbamate complexes have been reported to undergo clean thermal decomposition with little or no impurities [27]. In addition, the easy functionalization of dithiocarbamates offers innovative possibilities for the preparation of different structures, and this offers wide versatility in the synthesis of materials of nanometric dimension.

Herein, a quick, convenient and simple route to the preparation of PbS nanostructures by microwave irradiation in ethylene glycol is presented. The ethylene glycol acted a dual role as solvent and as passivating molecule which controlled the particle size and morphology of PbS nanoparticles. The products were characterized using absorption spectroscopy, X-ray powder diffraction (XRD), and transmission electron microscopy (TEM).

2. Experimental

2.1. Materials and physical measurements

All reagents and solvents were analytical grade and used as received without further purification. Elemental analysis for C, H, N and S were carried out on Elementar, Vario EL Cube, set up for CHNS analysis. The FTIR spectra were obtained using a Bruker alpha-P FTIR in the frequency range 4000−400 cm^{-1}. A 600 MHz Bruker Avance III NMR spectrometer was used to obtain the ^{1}H and ^{13}C NMR spectra at room temperature, using $CDCl_3$ as a solvent and TMS as an internal reference. Thermal analysis was performed using TGA 7 fitted with a thermal analysis controller (TAC 7/DX). Powder X-ray diffraction patterns were recorded using Röntgen PW3040/60 X'Pert Pro X-ray diffractometer with Ni-filtered Cu Ka radiation ($\lambda = 1.5405$ A). Absorption spectra were recorded on Perkin-Elmer λ20 UV-vis spectrophotometer. TEM measurement was by TECNAI G2 (ACI) instrument.

2.2. Synthesis of Lead(II) bis(*N*-ethyl-*N*-phenyldithiocarbamate), (1)

A mixture of N-ethylaniline (152 mg, 1.25 mmol) and ammonium hydroxide (7.5 mL) was stirred in an ice bath for 15 min. To this solution, carbon disulphide

https://doi.org/10.1016/j.heliyon.2019.e01413

(1.25 mmol) was added and stirred vigorously. After 45 min, lead(II) nitrate (207 mg, 0.625 mmol) in water (25 mL) was added dropwise with stirring resulting in a creamy white precipitate. The mixture was further stirred for 45 min, and the product obtained was filtered, washed with ethanol-water (1:3) mixture, and dried.

Yield: 87%, Mp = 200−201 °C. Selected FTIR, υ(cm^{-1}): 1470 (C=N), 1210 (C_2−N), 952 (C=S). ^{1}H NMR ($CDCl_3$) δ = 4.14 (q, -CH_2), 1.25 (t, -CH_3), 7.25−7.41 (m, C_6H_5). ^{13}C NMR ($CDCl_3$) d = 54.24 (-CH_2), 12.35 (-CH_3), 126.95, 128.28, 129.41, 145.13 (C_6H_5), 206.88 (CS_2). Anal. Calc. (%) for $C_{18}H_{20}N_2S_4Pb$ (599.82): C: 36.04; H: 3.36; N: 4.67; S: 21.38. Found (%): C: 36.20; H: 3.47; N: 5.01; S: 21.48.

2.3. Synthesis of Lead(II) bis(*N*-butyl-*N*-phenyldithiocarbamate), (2)

N-butylaniline (190 mg, 1.25 mmol) was mixed with ammonium hydroxide (7.5 mL) and cooled in an ice bath. To this solution was added carbon disulphide (1.25 mmol), and stirred for 45 min resulting into a yellowish-orange solution. A 25 mL aqueous solution of lead(II) nitrate (207 mg, 0.625 mmol) was added dropwise resulting in a creamy white precipitate. The mixture was further stirred for 45 min, and the precipitate was collected by filtration and washed with ethanol-water (1:3) mixture and dried.

Yield: 81%, Mp = 166−168 °C. Selected FTIR, υ(cm^{-1}): 1472 (C=N), 1218 (C_2−N), 955 (C=S). ^{1}H NMR ($CDCl_3$) δ = 4.06 (q, α-CH_2), 1.68 (m, β-CH_2), 1.30 (m, γ-CH_2), 0.87 (t, d-CH_3), 7.22−7.40 (m, C_6H_5). ^{13}C NMR ($CDCl_3$) d = 56.73 (α- CH_2), 29.55 (β-CH_2), 20.36 (γ-CH_2), 14.12 (d-CH_3), 127.90, 128.48, 129.80, 144.17 (C_6H_5), 206.64 (CS_2). Anal. Calc. for $C_{22}H_{28}N_2S_4Pb$ (655.93): C, 40.28; H, 4.30; N, 4.27; S, 19.55. Found: C, 40.18; H, 4.22; N, 4.28; S, 20.05%.

2.4. Synthesis of PbS nanostructures

In a typical microwave procedure, about 0.5 mmol of the Pb(II) dithiocarbamate was dispersed in 20 mL ethylenediamine and sonicated for 20 min to obtain a homogenous dispersion. The reaction mixture was transferred into a teflon sealed can and heated in a microwave oven (Multiwave 3000 microwave sample system, Anton Paar, Synthos) holding at a power of 800 W for 2 min, with stirring. After cooling the solution to room temperature naturally, the dark brown products formed were isolated by centrifugation, washed several times with absolute ethanol and dried at 50 °C overnight.

https://doi.org/10.1016/j.heliyon.2019.e01413

3. Results and discussion

3.1. Spectroscopic studies

The FTIR spectra of complexes (**1**) and (**2**) showed vibrational frequencies at 1470 and 1472 cm^{-1} respectively, which were attributed to the C═N stretching vibration of dithiocarbamate compounds. These bands were indicative of partial double bond character of the C-N stretching vibration [28]. The single symmetric peak observed around 954 cm^{-1} was the stretching vibration of (C-S) and suggested a bidentate mode of coordination in both compounds [29]. The peaks around 3150 cm^{-1} were due to the (=C-H) of the aromatic ring.

The NMR spectra of complexes (**1**) and (**2**) are shown in Figs. 1 and 2 respectively. The protons of the aromatic ring resonated in the low field region as multiplets in the range 7.25−7.41 ppm and 7.22−7.40 ppm for complexes (**1**) and (**2**) respectively [29]. The signals due to the methylene protons ($-CH_2$) appeared as a quartet at 54.24 ppm in the spectra of complex (**1**), and at 4.06, 1.68 and 1.30 ppm in the spectra of complex (**2**) due to the longer chain length of the butyl group. The position of the resonant frequencies of the methyl groups in both complexes, depicts their proximity to the electronegative N-atom and the thioureide moiety [29]. While the methyl protons of complex (**1**) resonated at 1.25 ppm, the methyl protons of complex (**2**) appeared at 0.87 ppm due to its distance from the deshielding effect of the nitrogen. In the ^{13}C NMR spectra, both complexes showed signals around 206 ppm which was ascribed to the quaternary carbon of the thioureide group [30]. The signals due to the aromatic carbons resonated in the range 126−145 ppm in the spectra of both complexes.

3.2. Thermal decomposition studies

The application of microwave irradiation to the preparation of nanoparticles via the breakdown of compounds is attributed to its unique rapid volumetric heating, which results into dramatic increase in reaction rates. Thus, since this proceeds via thermal decomposition reaction, the thermogravimetric analysis of the compounds was carried out.

The superimposed TGA/DTG curves for complexes 1 and 2 are presented in Fig. 3a and b respectively. The thermal analysis showed only one-step decomposition in both compounds. They are very stable showing decomposition started above 250 °C, after melting at 198 °C (complex 1) and 165 °C (complex 2). The graphs indicated that both complexes maintained their stability for another 100 °C, before decomposition began, and they exhibited sharp one step decomposition with about 65% weight loss, without the formation of thiocyanate intermediate, to give PbS (expmt. 1.98, calcd. 2.01 mg) as a final residue. The formation of isothiocyanate as an intermediate product in the thermal decomposition of dithiocarbamate

https://doi.org/10.1016/j.heliyon.2019.e01413

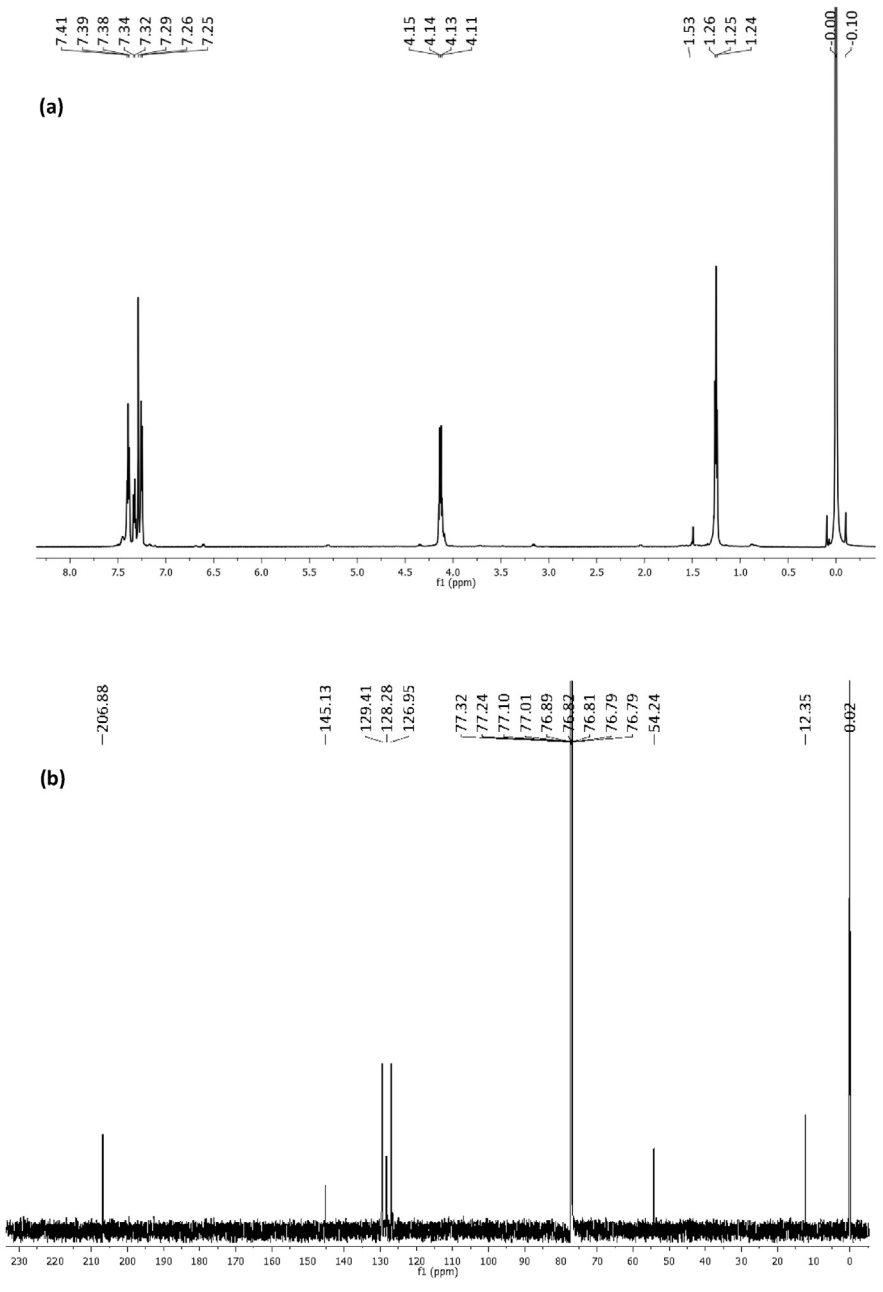

Fig. 1. (a) ^{1}H and (b) ^{13}C NMR spectra of complex 1.

complexes is well reported [31, 32, 33]. The maximum rate of decomposition for this step occurred at 346 and 344 °C for complexes 1 and 2 respectively. The overlapped TG curves of both complexes are shown in Fig. 3c, while the overlapped DTG are presented in Fig. 3d. Both Figures confirmed the close thermal stability of both compounds. The decomposition profile of precursor compounds is very important in material synthesis because it influences the shape and size of the nanoparticles obtained. However, due to the similarity in the decomposition patterns of these two

https://doi.org/10.1016/j.heliyon.2019.e01413

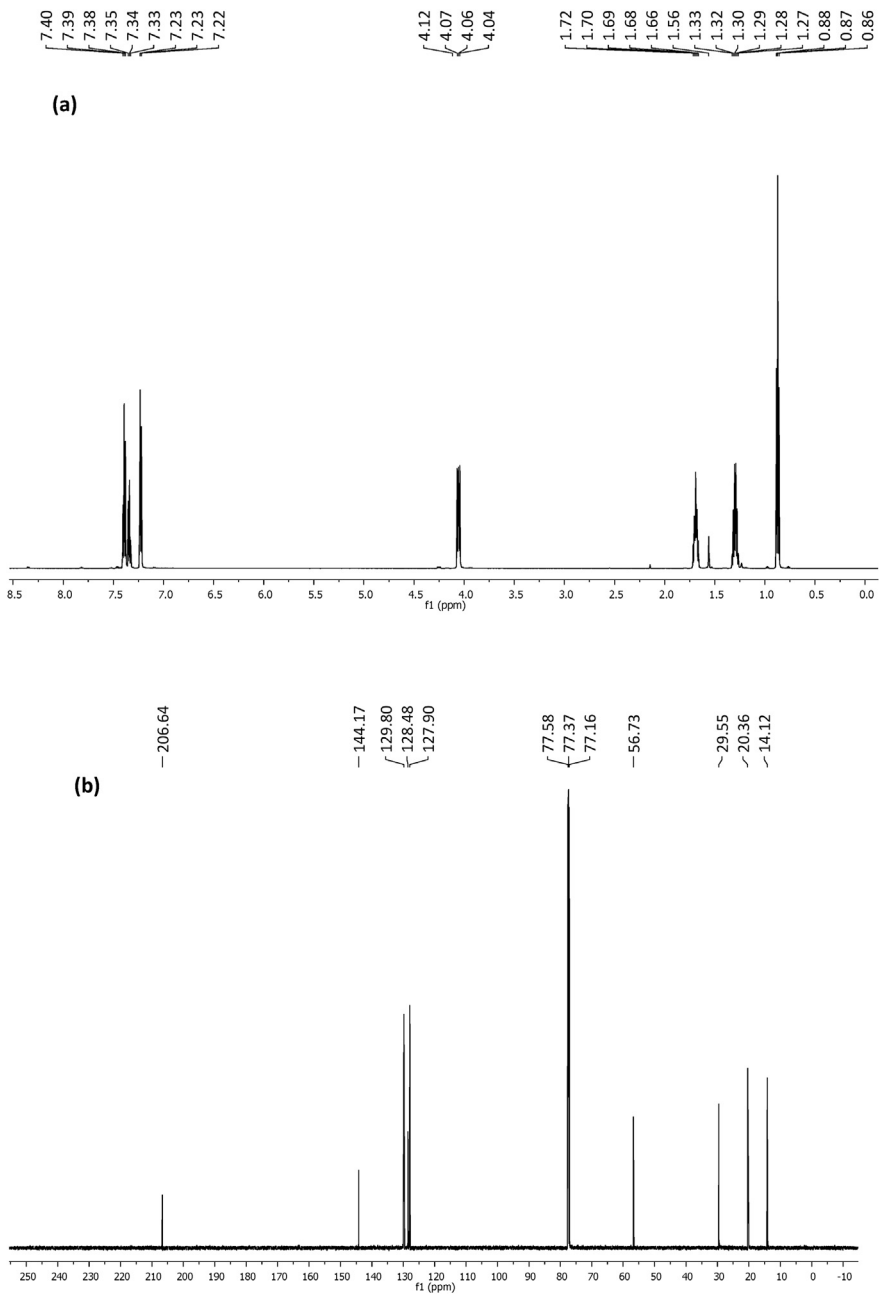

Fig. 2. (a) ^{1}H and (b) ^{13}C NMR spectra of complex 2.

compounds, variation in the morphology and size of their products may be governed by parameters other than decomposition behaviour.

3.3. The XRD studies

The X-ray diffraction patterns of the PbS are shown in Fig. 4(a and b). The patterns corresponded to the (1 1 1), (2 0 0), (2 2 0), (3 1 1), (2 2 2), (4 0 0), (3 3 1), (4 2 0)

https://doi.org/10.1016/j.heliyon.2019.e01413

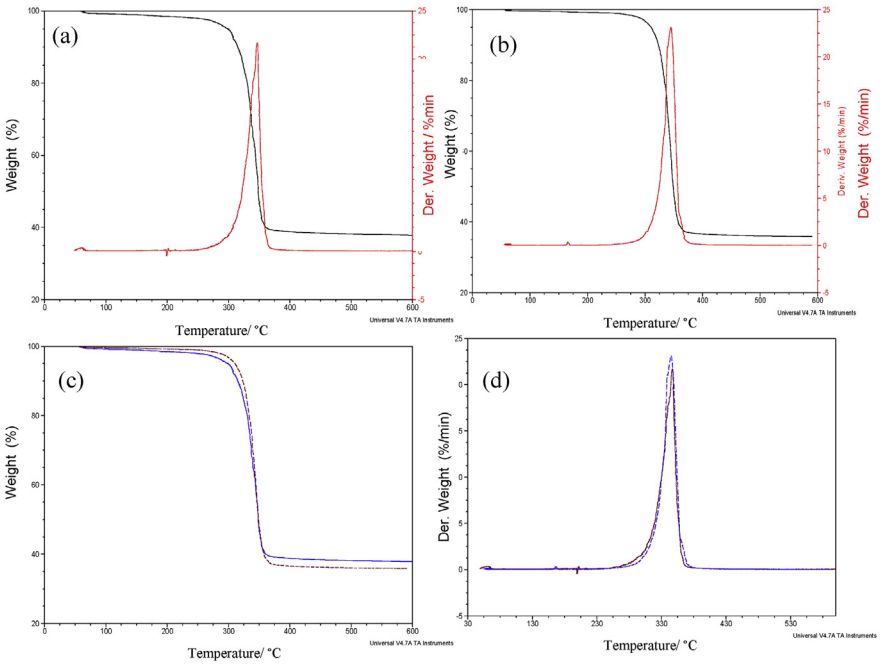

Fig. 3. TGA-DTG of (a) complex 1, (b) complex 2; and overlapped (c) TGA (d) DTG of complexes 1 and 2.

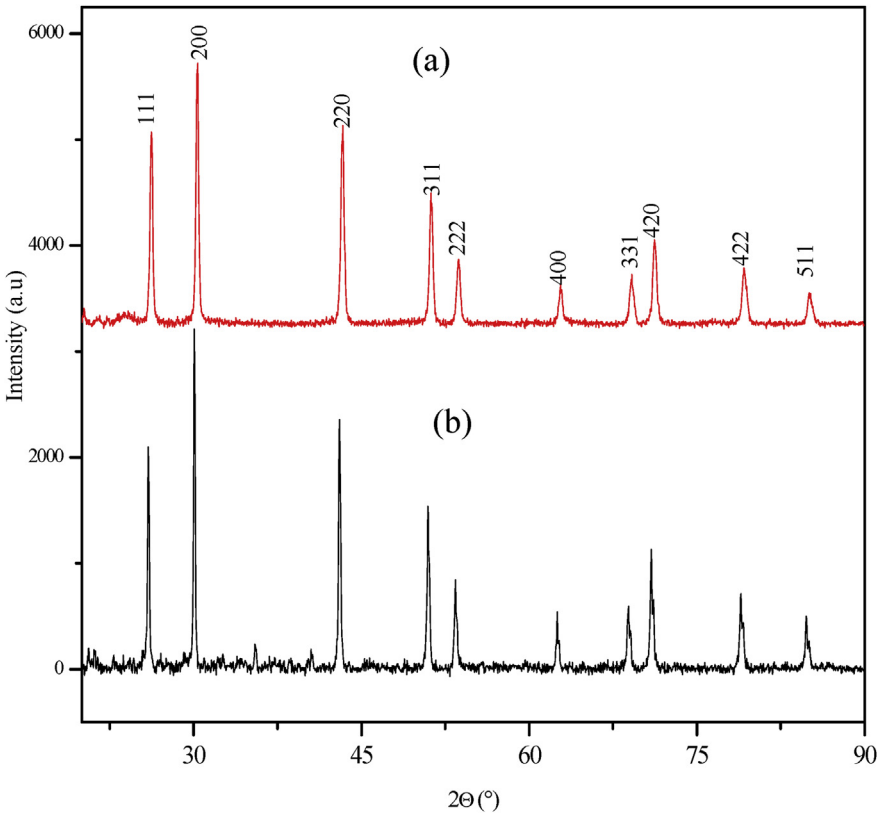

Fig. 4. XRD pattern for PbS synthesised under microwave irradiation using (a) complex 1 and (b) complex 2 as precursor compounds.

https://doi.org/10.1016/j.heliyon.2019.e01413

and (4 2 2) reflections of cubic Galena, PbS, (JCPDS No. 00-005-0592). The high crystallinity of the samples was demonstrated in the sharpness of the peaks. The patterns showed fairly complete decomposition of the precursor compounds resulting into PbS. The XRD peak of all the samples showed that the intensity of the (2 0 0) peaks were higher than to that of the (1 1 1) peaks. This indicates that the growth rate on the (1 0 0) facets was higher than the (1 1 1) facets [34]. The similarity of the patterns in the samples obtained from the two precursors is an indication that the difference in the compounds did not alter the growth pattern on the (1 0 0) facets compared to the (1 1 1) facets. However, the variation in the peak intensities may result into changes of morphological properties. The p-XRD of PbS nanoparticles synthesized using lead ethyl xanthogenate complex as single source precursor in a solution of ionic liquid, as capping agent, has been reported at two different temperatures; and both yielded pure cubic rock salt phase of PbS nanoparticles [35]. The crystal growth of the nanoparticles showed preference towards the (2 0 0) plane for the samples obtained at 150 °C. However, with increased temperature to about 200 °C, the (2 2 0) growth orientation was preferred, with the formation of more crystalline nanoparticles.

3.4. TEM studies

Figs. 5a and 6a show the TEM images of the PbS nanostructures obtained using complexes 1 and 2 respectively. The effect of different complexes (under same synthesis conditions) on the morphology and size of the obtained PbS nanostructures is very conspicuous. The TEM images of PbS nanostructures prepared from complex 1 are shown in Fig. 5a and b. The images showed PbS nanorods with irregular length and average diameter of 33 nm. Fig. 5c and d are the HRTEM, showing the lattice fringes, and SAED images of the nanorods respectively, which confirmed the high crystallinity of the prepared PbS. The nanostructures from complex 2 have non-uniform cube-like shape with 150 nm as average length of sides as shown in Fig. 6b. The shape of nanoparticles is dependent on nucleation and growth process. In microwave synthesis, solvents play a critical role in the process of products formation. Properties such as the rate of collision between the reactants molecules, the rate of heating of the reaction, and the reaction temperature vary in different solvents. Therefore, different nanostructures would result from different solvents. However, in the synthesis of nanoparticles using precursor compounds, the properties of the compounds have significant influence on their morphology and size. More specifically, in dithiocarbamate slight variation in the functional groups on the dithiocarbamato ligand have pronounced influence on the properties of the resulting nanoparticles even at uniform synthesis conditions such as temperature and solvent.

The growth mechanism determines the shape of nanostructures obtained and their phases. During the process of nucleation, all nanoparticles tend to produce a face

https://doi.org/10.1016/j.heliyon.2019.e01413

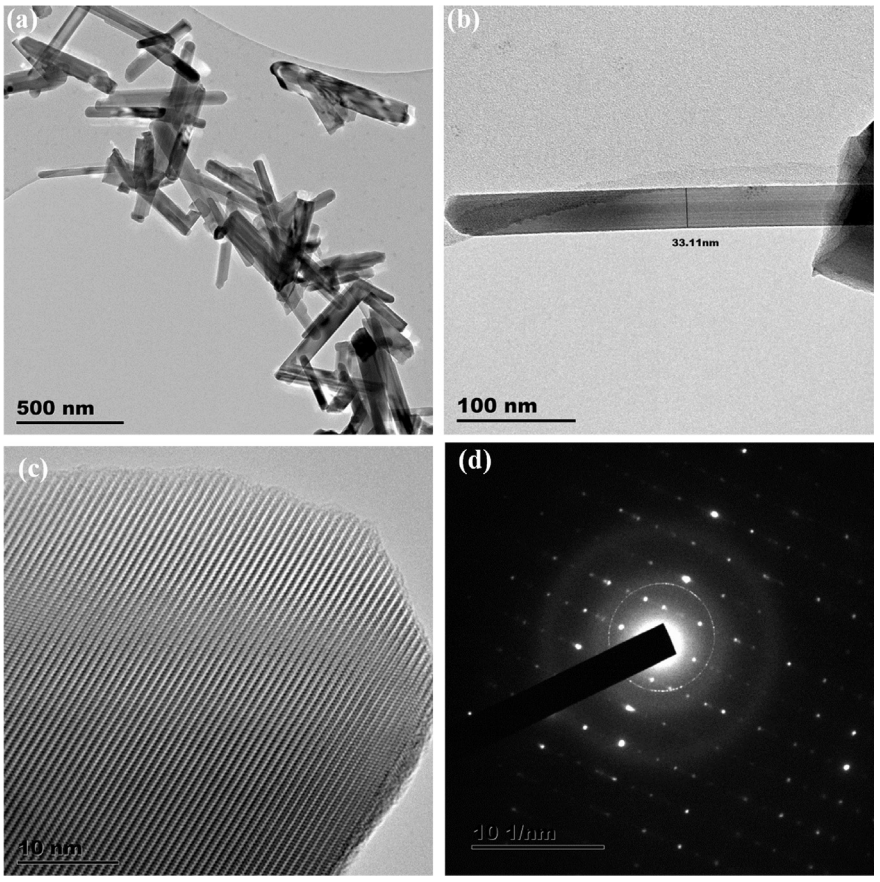

Fig. 5. (a) and (c) TEM images of PbS and their corresponding (b) HRTEM and (d) SAED PbS nanorods synthesized from complex 1.

centred cubic (FCC) phase. Thus, the ratio of the relative growth rate of (111) and (100) directions within the initial truncated octahedron seed is the major determinant of the final shape of the nanocrystals. The major factors reported to govern the growth rates include the reaction temperature, time, precursor concentration and the type of capping agent used [34]. Capping groups are capable of adsorbing onto the [100] plane, thereby allowing growth along the [111] plane [36]. The anion ligand polyhedron, Pb-S_6 octahedron, is the major growth element in pure PbS [34]. According to Pauling rules, the octahedrons are coherently coupled on the (111) facets sharing one edge. These facets posses better stability than the (100) facets, and are responsible for the growth rate of the (111) being slightly higher than the rate observed in the (100) facets [34].

Therefore, in the present studies the formation of the PbS rods in ethylene glycol may be due to the selective binding to the specific crystallite facets of the PbS through the hydroxyl groups of ethylene glycol. This process selectively stabilized the (111) face of PbS, resulting in anisotropic growth along the (100) face [37]. Furthermore, the formation of various morphologies in the synthesis of nanoparticles

https://doi.org/10.1016/j.heliyon.2019.e01413

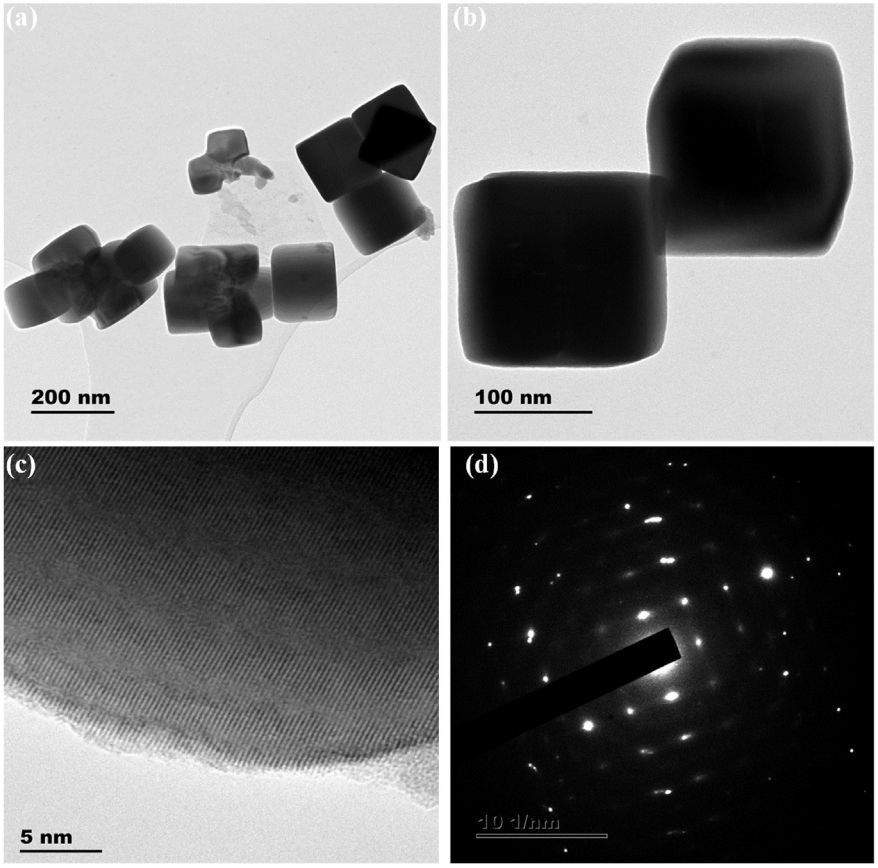

Fig. 6. (a) and (c) TEM images of PbS and their corresponding (b) HRTEM and (d) SAED PbS nanocubes synthesized from complex 2.

using the single source precursor route has been largely attributed to the size and functional groups of the ligands present in the precursor compounds [23, 38]. Among several other factors, Peng *et al.*, reported that the nature of the precursor is also one of the factors that influence the particle morphology [39, 40]. Complex (2) possesses longer alkyl group and would tend to last longer as a result of high steric hindrance [41]. This may facilitate the growth of different morphology of PbS nanostructure compared to lower alkyl group ligand of complex (1). The formation of cubes when complex (2) was used may have originated from the formation of a thermodynamically cubic center [42]. The distinct lattice fringes in the HRTEM of Fig. 6c and the selective area electron diffraction (SAED) pattern in 6d confirmed the formation of crystalline PbS nanostructures from precursor complex 2.

3.5. UV-vis-NIR spectral properties

The UV-vis-NIR absorption spectra of the PbS nanostructures obtained using complexes 1 and 2 at different irradiation times are shown in Fig. 7a and b respectively. The graphs show that remarkable changes occurred in the spectra of the

https://doi.org/10.1016/j.heliyon.2019.e01413

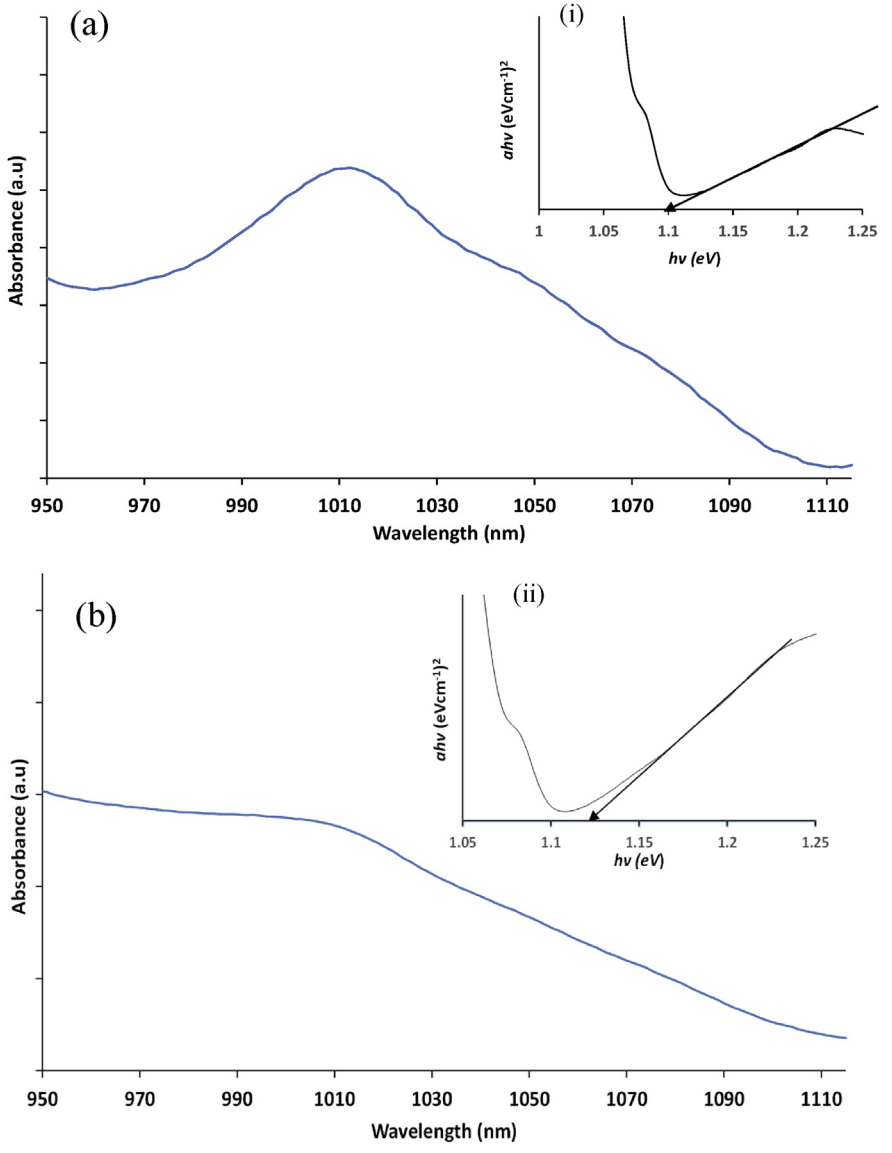

Fig. 7. Absorption spectra of PbS obtained from (a) complex 1 and (b) complex 2, and their respective Tauc plot in the inserts (i) and (ii).

nanostructures obtained from the two precursor compounds. The excitonic peak in both spectra is centred on 1010 nm (1.22 eV). The absorption spectrum of the nanoparticles grown from complex 1 showed pronounced excitonic peak which broadened in the spectrum of complex 2. Generally, the position of absorption peak and the spectral shape are both dependent on different properties of the particles such as concentration, their size and the distribution. These 3 properties are controlled by the processes of nucleation and crystal growth which occurred during the synthesis process. However, the process of nucleation and crystal growth are largely affected by the type of precursor used for the particles' synthesis. The

https://doi.org/10.1016/j.heliyon.2019.e01413

concentration of the nanostructures, size and distribution are also significantly affected by the duration of the microwave irradiation [42]. The band gap of the nanostructures was determined from the Tauc plot in the insert. The Tauc function is based on the relationship which exists between absorption coefficient (α) and photon energy ($h\nu$); and is given in Eq. (1) [43]:

$$\alpha h\nu = A(h\nu - E_g)^n, \quad (1)$$

where E_g is the optical band gap which corresponds to transitions indicated by the value of n. The value of n is 1/2, 3/2, 2, and 3 for direct allowed and forbidden transitions, and indirect allowed and forbidden transitions, respectively. In this case, ($n = 2$, direct) [44]. The optical band gaps of the PbS from complexes 1 and 2 were found to be 1.10 and 1.12 eV respectively. These indicated significant shift to shorter wavelengths with respect to the bulk material (0.4 eV) [45].

4. Conclusion

Novel Pb(II) dithiocarabamte complexes have been utilised as single source precursors to synthesize PbS nanostructures by microwave irradiation technique. The results show that the precursor type has significant effect on the morphology, size and optical properties of the PbS nanostructures. The prepared nanostructures ranged from rods to cubic shapes. It is suggested that this facile microwave irradiation route to PbS nanorods and nanocubes could also be used for the synthesis of nanostructures of other technologically important chalcogenide semiconductors.

Declarations

Author contribution statement

Damian Onwudiwe: Conceived and designed the experiments; Performed the experiments; Analyzed and interpreted the data; Contributed reagents, materials, analysis tools or data; Wrote the paper.

Funding statement

This research did not receive any specific grant from funding agencies in the public, commercial, or not-for-profit sectors.

Competing interest statement

The authors declare no conflict of interest.

Additional information

No additional information is available for this paper.

https://doi.org/10.1016/j.heliyon.2019.e01413

References

[1] T. Ding, J.-R. Zhang, S. Long, J.-J. Zhu, Synthesis of HgS and PbS nanocrystals in a polyol solvent by microwave heating, Microelectron. Eng. 66 (2003) 46−52.

[2] S.A. Empedocles, Influence of spectral diffusion on the line shapes of single CdSe nanocrystallite quantum dots, J. Phys. Chem. B 103 (11) (1999) 1826−1830.

[3] B. Ludolph, M.A. Malik, P. O'Brien, N. Revaprasadu, Novel single molecule precursor routes for the direct synthesis of highly monodispersed quantum dots of cadmium or zinc sulfide or selenide, Chem. Commun. 17 (1998) 1849−1850.

[4] A.K. Dutta, T. Ho, L. Zhang, P. Stroeve, Nucleation and growth of lead sulfide nano- and microcrystallites in supramolecular polymer assemblies, Chem. Mater. 12 (2000) 1042−1048.

[5] F. Davar, M. Mohammadikish, M.R. Loghman-Estarki, M. Masteri-Farahani, Synthesis of micro-and nanosized PbS with different morphologies by the hydrothermal process, Ceram. Int. 40 (2014) 8143−8148.

[6] Z.Q. Mamiyev, N.O. Balayeva, Preparation and optical studies of PbS nanoparticles, Opt. Mater. 46 (2015) 522−525.

[7] Y. Wang, Nonlinear optical properties of nanometer-sized semiconductor clusters, Acc. Chem. Res. 24 (1991) 133−139.

[8] S.K. Goswami, E. Oh, Morphology control and photovoltaic application of solvothermally synthesized PbS nanostructures, Mater. Lett. 117 (2014) 138−141.

[9] Z. Zhao, J. Zhang, F. Dong, B. Yang, Supercrystal structures of polyhedral PbS nanocrystals, J. Colloid Interface Sci. 359 (2011) 351−358.

[10] J. Zhu, S. Liu, O. Palchik, Y. Koltypin, A. Gedanken, A novel sonochemical method for the preparation of nanophasic sulfides: synthesis of HgS and PbS nanoparticles, J. Solid State Chem. 153 (2000) 342−348.

[11] Z. Zhao, K. Zhang, J. Zhang, K. Yang, C. He, F. Dong, B. Yang, Synthesis of size and shape controlled PbS nanocrystals and their self-assembly, Colloids Surf. A Physicochem. Eng. Asp. 355 (2010) 114−120.

[12] D. Kumar, G. Agarwal, B. Tripathi, D. Vyas, V. Kulshrestha, Characterization of PbS nanoparticles synthesized by chemical bath deposition, J. Alloys Compd. 484 (2009) 463−466.

https://doi.org/10.1016/j.heliyon.2019.e01413

[13] Q. Zhengping, X. Yi, Z. Yingjie, Q. Yitai, Synthesis of PbS/poly(vinyl acetate) nanocomposites by γ-irradiation, Mater. Sci. Eng. B 77 (2000) 144−146.

[14] C.Y. Wang, X. Mo, Y. Zhou, Y.R. Zhu, H.T. Liu, Z.Y. Chen, A convenient ultraviolet irradiation technique for in situ synthesis of CdS nanocrystallites at room temperature, J. Mater. Chem. 10 (2000) 607−608.

[15] M. Kowshik, W. Vogel, J. Urban, S.K. Kulkarni, K.M. Paknikar, Microbial synthesis of semiconductor PbS nanocrystallites, Adv. Mater. 14 (2002) 815−818.

[16] H. Yin, T. Yamamoto, Y. Wada, S. Yanagida, Large-scale and size-controlled synthesis of silver nanoparticles under microwave irradiation, Mater. Chem. Phys. 83 (2004) 66−70.

[17] Z.P. Qiao, Y. Zhang, L.T. Zhou, Q. Xire, Shape control of PbS crystals under microwave irradiation, Cryst. Growth Des. 7 (2007) 2394−2396.

[18] J.H. Warner, Self-assembly of ligand-free PbS nanocrystals into nanorods and their nanosculpturing by electron-beam irradiation, Adv. Mater. 20 (2008) 784−787.

[19] P. Zhao, G. Chen, Y. Hu, X. liang He, K. Wu, Y. Cheng, K. Huang, Preparation of dentritic PbS nanostructures by ultrasonic method, J. Cryst. Growth 303 (2007) 632−637.

[20] J.-Q. Sun, X.-P. Shen, L.-J. Guo, K.-M. Chen, Q. Liu, Microwave-assisted synthesis of flower-like PbS crystals, Phys. E Low Dimens. Syst. Nanostruct. 41 (2009) 1527−1532.

[21] D. Ondrušová, M. Pajtášová, E. Jóna, M. Koman, Structural properties of Co(III), Hg(II) and Pb(II) N-ethyl-N-phenyl-dithiocarbamates and their application in the rubber industry, Solid State Phenom. 90−91 (2003) 383−388.

[22] L.D. Nyamen, V.S. Rajasekhar Pullabhotla, A.A. Nejo, P. Ndifon, N. Revaprasadu, Heterocyclic dithiocarbamates: precursors for shape controlled growth of CdS nanoparticles, New J. Chem. 35 (2011) 1133−1139.

[23] L.D. Nyamen, N. Revaprasadu, R.V.S.R. Pullabhotla, A.A. Nejo, P.T. Ndifon, M.A. Malik, P. O'Brien, Synthesis of multi-podal CdS nanostructures using heterocyclic dithiocarbamato complexes as precursors, Polyhedron 56 (2013) 62−70.

[24] W.N. Kun, S. Mlowe, L.D. Nyamen, P.T. Ndifon, M.A. Malik, O.Q. Munro, N. Revaprasadu, Heterocyclic bismuth(III) dithiocarbamato complexes as single-source precursors for the synthesis of anisotropic Bi_2S_3 nanoparticles, Chem. Eur. J. 22 (2016) 13127−13135.

https://doi.org/10.1016/j.heliyon.2019.e01413

[25] S.A. Saah, M.D. Khan, P.D. McNaughter, J.A.M. Awudza, N. Revaprasadu, P. O'Brien, Facile synthesis of a $PbS_{1-x}Se_x$ ($0 \leq x \leq 1$) solid solution using bis(N,N-diethyl-N - naphthoylchalcogenoureato)lead(II) complexes, New J. Chem. 42 (2018) 16602−16607.

[26] M.D. Khan, S. Hameed, N. Haider, A. Afzal, M.C. Sportelli, N. Cioffi, M.A. Malik, J. Akhtar, Deposition of morphology-tailored PbS thin films by surfactant-enhanced aerosol assisted chemical vapor deposition, Mater. Sci. Semicond. Proc. 46 (2016) 39−45.

[27] A. Roffey, N. Hollingsworth, H.-U. Islam, M. Mercy, G. Sankar, C.R.A. Catlow, G. Hogarth, N.H. de Leeuw, Phase control during the synthesis of nickel sulfide nanoparticles from dithiocarbamate precursors, Nanoscale 8 (2016) 11067−11075.

[28] D.C. Onwudiwe, P.A. Ajibade, Synthesis and characterization of metal complexes of N-alkyl-N-phenyl dithiocarbamates, Polyhedron 29 (2010) 1431−1436.

[29] F.F. Bobinihi, J. Osuntokun, D.C. Onwudiwe, Syntheses and characterization of nickel(II) dithiocarbamate complexes containing NiS_4 and NiS_2PN moieties: nickel sulphide nanoparticles from a single source precursor, J. Saudi Chem. Soc. 22 (2018) 381−395.

[30] D.C. Onwudiwe, P.A. Ajibade, Synthesis and characterization of Zn(II), Cd(II) and Hg(II) alkyl-aryl dithiocarbamate: X-ray crystal structure of $[(C_6H_5N(et)CS_2)Hg(C_6H_5N(butyl)CS_2)]$, Synth. React. Inorg. Met. Nano Metal Chem. 40 (2010) 279−284.

[31] N. Hollingsworth, A. Roffey, H.-U. Islam, M. Mercy, A. Roldan, W. Bras, M. Wolthers, C.R.A. Catlow, G. Sankar, G. Hogarth, N.H. de Leeuw, Active nature of primary amines during thermal decomposition of nickel dithiocarbamates to nickel sulfide nanoparticles, Chem. Mater. 26 (2014) 6281−6292.

[32] L.A. Ramos, É.T.G. Cavalheiro, Preparation, characterization and thermal decomposition of sodium and potassium salts of dithiocarbamate, Braz. J. Therm. Anal. 2 (2013) 38.

[33] J.O. Hill, S. Chirawongaram, Thermal analysis studies of tin dithiocarbamate complexes − a short review, J. Therm. Anal. 41 (1994) 511−518.

[34] M. Liu, W. Li, Growth and optical property of PbS/ZnS nanocrystals, Superlattic. Microstruct. 120 (2018) 727−731.

https://doi.org/10.1016/j.heliyon.2019.e01413

[35] Z. Tshemese, M.D. Khan, S. Mlowe, N. Revaprasadu, Synthesis and characterization of PbS nanoparticles in an ionic liquid using single and dual source precursors, Mater. Sci. Semicond. Proc. 227B (2018) 116−121.

[36] G.B. Shombe, E.B. Mubofu, S. Mlowe, N. Revaprasadu, Synthesis of hierarchical PbS nanostructures capped with castor oil, Mater. Lett. 185 (2016) 17−20.

[37] J.W. Kyobe, E.B. Mubofu, Y.M.M. Makame, S. Mlowe, N. Revaprasadu, CdSe quantum dots capped with naturally occurring biobased oils, New J. Chem. 39 (2015) 7251−7259.

[38] K.P. Mubiayia, N. Revaprasadu, S.S. Garje, M.J. Moloto, Designing the morphology of PbS nanoparticles through a single source precursor method, J. Saudi Chem. Soc. 21 (2017) 593−598.

[39] X. Peng, Mechanisms for the shape-control and shape-evolution of colloidal semiconductor nanocrystals, Adv. Mater. 15 (2003) 459−463.

[40] Z.A. Peng, X. Peng, Nearly monodisperse and shape-controlled CdSe nanocrystals via alternative routes: nucleation and growth, J. Am. Chem. Soc. 124 (2002) 3343−3353.

[41] H.M. Irving, R.J. Williams, The stability of transition-metal complexes, J. Chem. Soc. (1953) 3192−3210.

[42] D. Kuang, A. Xu, Y. Fang, H. Liu, C. Frommen, D. Fenske, Surfactant-assisted growth of novel PbS dendritic nanostructures via facile hydrothermal process, Adv. Mater. 15 (2003) 1747−1750.

[43] H. Li, L. Chai, X. Wang, X. Wu, G. Xi, Y. Liu, Y. Qian, Hydrothermal growth and morphology modification of β-NiS three-dimensional flowerlike architectures, Cryst. Growth Des. 7 (2007) 1918−1922.

[44] M.H. Patel, T.K. Chaudhuri, V.K. Patel, T. Shripathi, U. Deshpande, N.P. Lalla, Dip-coated PbS/PVP nanocomposite films with tunable band gap, RSC Adv. 7 (2017) 4422−4429.

[45] G.I. Koleilat, L. Levina, H. Shukla, S.H. Myrskog, S. Hinds, A.G. Pattantyus-Abraham, E.H. Sargent, Efficient, stable infrared photovoltaics based on solution-cast colloidal quantum dots, ACS Nano 2 (2008) 833−840.

https://doi.org/10.1016/j.heliyon.2019.e01413